RSC Advances

PAPER

View Article Online
View Journal | View Issue

Cite this: *RSC Adv.*, 2017, **7**, 36403

Polyaniline–single walled carbon nanotube composite – a photocatalyst to degrade rose bengal and methyl orange dyes under visible-light illumination†

Mukulika Jana Chatterjee,[a] Amrita Ghosh,[b] Anup Mondal[b] and Dipali Banerjee *[a]

The polyaniline/single walled carbon nanotube (PANI–SWCNT) composites were prepared by the polymerization of an aniline monomer in the presence of sulfosalicylic acid with SWCNT under *in situ* conditions. PANI and PANI–SWCNT composites were characterized by X-ray diffraction (XRD), field emission scanning electron microscopy (FESEM), ultra violet-visible spectroscopy (UV-Vis), Fourier transform infra-red spectroscopy (FTIR), X-ray photoelectron spectroscopy (XPS), photoluminescence spectroscopy (PL) and Brunauer–Emmett–Teller (BET) analysis. The application of the composites as a recyclable photocatalysts with visible-light-driven photocatalytic activity and photostability for the degradation of organic dyes – Rose Bengal (RB) and Methyl Orange (MO) – is demonstrated. PANI–SWCNT composite, with 2 weight% SWCNT content, has emerged as the best with degradation efficiencies of 95.91% and 90.34% against the performance of PANI with degradation efficiencies of 85.2% and 75.9% for RB and MO within 10 and 30 minutes, respectively. The synergistic effect between PANI and SWCNT is found to impart improved photogenerated carrier separation in the composite. A possible photocatalytic mechanism on the enhancement of the visible light performance of the composite over pure PANI is discussed based on the results of an active species trapping experiment.

Received 4th April 2017
Accepted 13th July 2017

DOI: 10.1039/c7ra03855k

rsc.li/rsc-advances

1. Introduction

Hazardous dyes are used worldwide with ever growing demand in sectors like printing, textiles, automobiles and other industries. These non-biodegradable organic dyes that are discharged from industries are the main contaminants in wastewater and are potentially harmful to mankind and other living animals. So it is a challenge to develop efficient techniques for dye removal from wastewater to maintain the ecosystem and environment.[1]

Recently combinations of conjugated polymers with inorganic or carbon based materials for enhanced visible light responsive photocatalysis have emerged as a significant area of research. Some such photocatalysts used for degradation of various dyes in recent past are as follows: graphene–polyaniline (Gr–PANI),[2] and aluminium doped zinc oxide polyaniline hybrids (Al doped ZnO–PANI)[3] for Rose Bengal dye (RB), Al doped ZnO–PANI hybrids,[3] titanium dioxide–polyaniline (TiO_2–PANI),[4] PANI-modified TiO_2 composite,[5] polypyrrole (PPY)–TiO_2,[6] polythiophene/titanium dioxide,[7] polythiophene/TiO_2,[8] PANI–Cr_3O_4 [9] for methyl orange dye (MO), PANI and ZnO nanocomposite,[10] PANI–ZnO,[11] zinc oxide *via* hybridization with monolayer polyaniline,[12] TiO_2 modified by PANI,[13] polyaniline modified TiO_2,[14] TiO_2/polyaniline composites,[15] silver (Ag)–TiO_2–PANI,[16] Ag@TiO_2/PANI,[17] Ag/AgCl–polyaniline,[18] PANI–nickel ferrite composite,[19] PANI-*g*-C_3N_4,[20] PPY–TiO_2,[21] ZnO_2/polypyrrole[22] and poly(3,4-ethylenedioxythiophene) (PEDOT)–ZnO[23] for methylene blue dye (MB), Ag@TiO_2/PANI[17] and polyaniline–silver–silver phosphate (PANI–Ag–$AgPO_4$)[24] for brilliant blue dye, PANI–ZnO[11] for malachite green dye, ZnO_2/polypyrrole,[22] (PANI–Ag–$AgPO_4$),[24] spindle-like PANI/$BiVO_4$,[25] TiO_2 modified by PANI,[13] polyaniline modified TiO_2 [14] for rhodamine B, poly(pyrrole-*co*-aniline)-coated TiO_2/nanocellulose[26] for eosin yellow, spindle-like PANI/$BiVO_4$ [25] for phenol.

Among various conjugated polymers, PANI is a p-type material with high hole transporting ability[5,14] together with fast charge separation capability, slow charge recombination rate in electron transfer processes and stability.[3,12,15] Due to that PANI has many applications in catalytic and photocatalytic field.[13,25,27–32]

On the other hand, due to superior electronic and transport properties,[33] CNT and CNT based composites have also been explored as visible light photocatalysts for degradation of dyes like MO,[34] MB,[35] indigo carmine, congo red and orange G dyes,[36]

[a]*Department of Physics, Indian Institute of Engineering Science and Technology (IIEST), Shibpur, Howrah – 711103, West Bengal, India. E-mail: dipalibanerjeebesu@gmail.com*

[b]*Department of Chemistry, Indian Institute of Engineering Science and Technology (IIEST), Shibpur, Howrah – 711103, West Bengal, India*

† Electronic supplementary information (ESI) available. See DOI: 10.1039/c7ra03855k

alizarin yellow R,[37] eosin yellow[38] and for removal of Cr(VI) from aqueous solution.[39] In the formation of the composite, SWCNTs have particular advantage over MWCNTs due to the greater degree of interphase contact that can be accessed by the surface of the second component of the composite with the bundle of small individual SWCNTs.

Based on that, PANI–SWCNT composite is expected to have exclusive properties such as enhanced photocatalytic activity, high stability because of the synergism between the constituents. Accordingly this paper reports the comparative photocatalytic activity of PANI and PANI–SWCNT composites with varying percentages under visible sunlight irradiation for the degradation of RB and MO. Toxic to human skin and eyes, RB is known to be a heavily used dye in textile and printing industries,[2] having IUPAC name 4,5,6,7-tetrachloro-2′,4′,5′,7′-tetraiodofluorescein disodium salt ($C_{20}H_2Cl_4I_4Na_2O_5$), molecular weight 1017.64.

Another dye MO, having IUPAC name sodium 4-[[4-(dimethylamino)phenyl]diazenyl]benzenesulfonate ($C_{14}H_{14}N_3NaO_3S$), molecular weight 327.33, has mutagenic properties and hence very much toxic for living animals. Apart from conjugated polymer and carbon based composites which we have already mentioned, some other materials reported to have been explored for the degradation of RB under visible light illumination are – ZnO in the presence of metal ions,[40] Cu_7S_4 thin films,[41] Cu_7Te_4 thin films,[42] p-CuO/n-ZnO thin film heterojunction,[43] manganese dioxide (MnO_2).[44]

Similarly materials like, p-CuO/n-ZnO thin film heterojunction,[43] Cu(II) in presence of tartaric acid,[45] fluidized bed reactor loaded with cross-linked chitosan embedded nano-CdS,[46] carbonaceous adsorbent prepared from waste rubber tires

Table 1 Comparison of kinetic parameters using different photocatalysts under visible and ultraviolet (UV) light irradiation for the degradation of RB and MO dyes

Serial no.	Ref. no.	Name of the photocatalyst	Name of the dye	Irradiation source	Irradiation time	Degradation efficiency (%) and/or rate constant (min^{-1})
1	2	Graphene/polyaniline	RB	Visible	3 h	56%
2	3	Aluminium doped zinc oxide–polyaniline hybrids	RB	Visible	150 min	2.61×10^{-2} min^{-1}
3	40	ZnO (pH 8)	RB	Visible	180 min	5.53×10^{-3} min^{-1}
4	41	Cu_7S_4 thin films (in the presence of H_2O_2)	RB	Visible	3 h	81%
						1×10^{-2} min^{-1}
5	42	Cu_7Te_4 thin films (in the presence of H_2O_2)	RB	Visible	90 min	92%
6	43	p-CuO/n-ZnO thin film heterojunction	RB	Visible	150 min	92%
						1.40×10^{-2} min^{-1}
7	44	Manganese dioxide (MnO_2)	RB	Visible	150 min	2.39×10^{-2} min^{-1}
8	3	Aluminium doped zinc oxide–polyaniline hybrids	MO	Visible	150 min	1.77×10^{-2} min^{-1}
9	50	Polyaniline-hybrid defective ZnO	MO	UV	120 min	94%
						2.33×10^{-2} min^{-1}
10	4	TiO_2/polyaniline	MO	Visible	120 min	49.9%
						3.7×10^{-3} min^{-1}
				UV	120 min	92.9%
						2.35×10^{-2} min^{-1}
11	5	PANI-modified TiO_2 composite	MO	UV	125 min	81.3%
						4.14×10^{-2} min^{-1}
				Visible	6 h	21.5%
						8.7×10^{-3} min^{-1}
12	51	Carbon nanotubes doped TiO_2	MO	UV	80 min	4.93×10^{-2} min^{-1}
13	6	Polypyrrole–TiO_2	MO	Visible	160 min	9.31×10^{-3} min^{-1}
14	52	Poly(3-hexylthiophene)/TiO_2	MO	UV	150 min	92.7%
						1.86×10^{-2} min^{-1}
15	53	TiO_2 nanoparticles using a triboelectric nanogenerator	MO	UV	120 min	76%
16	54	Nanostructured TiO_2/ZnO heterojunctions	MO	UV	30 min	97%
17	55	Aqueous TiO_2 suspensions (at pH 2)	MO	UV	40 min	98.31%
18	56	TiO_2-coated activated carbon	MO	UV	100 min	89%
19	46	Fluidized bed reactor loaded with cross-linked chitosan embedded nano-CdS (pH 4)	MO	Visible	80 min	99%
						2.6×10^{-2} min^{-1}
20	49	PEDOT nanospindles	MO	UV	15 min	100%
				Visible	180 min	100%
21	43	p-CuO/n-ZnO thin film heterojunction	MO	Visible	150 min	81%
						1×10^{-2} min^{-1}
22	48	Au nanoparticles loaded graphitic carbon nitride nanosheets	MO	Visible	2.5 h	92.6%
23	45	Cu(II) in presence of tartaric acid (for pH 3)	MO	Visible	70 min	92%
24	57	TiO_2/graphene	MO	UV	60 min	85%

(WRT),[47] gold (Au) nanoparticles loaded graphitic carbon nitride nanosheets[48] and poly(3,4-ethylenedioxythiophene) (PEDOT)[49] have been used as photocatalysts for degradation of MO under visible light illumination. As a ready reference, irradiation time, degradation efficiency, rate constant and nature of the irradiated light for the degradation of RB and MO using different photocatalysts are tabulated in Table 1 for a clear comparison.

For the present work, the composites were prepared by *in situ* oxidative polymerization of aniline in presence of SWCNT. The degradation efficiency and the rate constant of PANI and various composites were evaluated and the later showed higher efficiency and rate constant than PANI. The PANI–SWCNT composite exhibits excellent photocatalytic performance through the charge carrier separation compared to other photocatalysts. A possible photocatalytic mechanism was proposed and the improved photocatalytic activity is attributed to the electron–hole separation caused by the synergistic effect between PANI and SWCNT.

2. Experimental

2.1. Materials used

Single-walled carbon nanotubes (SWCNTs) were procured from US Research Nanomaterials, Inc. General grade aniline monomer was purchased from Fisher Scientific, India. Ethanol, 5-sulfosalicylic acid (SSA) and ammonium persulfate (APS) were bought from Merck Chemicals. De-ionised water was obtained from Hydrolab, India. Methyl Orange (MO) and Rose Bengal (RB) dyes were acquired from Himedia, India. Sodium oxalate (SO) and *p*-benzoquinone (BQ) were procured from Fisher Scientific, India. Potassium persulfate ($K_2S_2O_8$) and *tert*-butanol (TBA) were obtained from Sigma Aldrich and SD Fine-Chem Limited (SDFCL), respectively.

2.2. Synthesis of PANI and PANI–SWCNT nanocomposite *via in situ* chemical polymerization technique

PANI–SWCNT nanocomposite was synthesized by *in situ* chemical oxidative polymerization process as described in our earlier work.[58] Aniline was added to an aqueous solution of SSA. Depending on the desired weight percentage content of SWCNTs in the composite, certain amounts of SWCNTs were added to the SSA mixed aniline solution and stirred for half an hour. Aqueous solution of APS was added drop by drop and after leaving for overnight, the blackish green precipitate was centrifuged and filtered out after rinsing with water and ethanol repeatedly. The samples were dried properly, powdered and used for the experiments.

SSA doped pure PANI was also synthesized in the same way as mentioned above without SWCNT and it is denoted as PSA. PANI–SWCNT nanocomposites containing three different weight percentages of SWCNT have been denoted as PC1 (1% SWCNT content), PC2 (2% SWCNT content) and PC4 (4% SWCNT content).

2.3. Characterization and measurements

The synthesized samples were characterized by powder X-ray diffraction spectroscopy (XRD), field emission scanning electron microscopy (FESEM), ultra violet and visible ray spectroscopy (UV-Vis), Fourier transform infrared spectroscopy (FTIR), X-ray energy photoelectron spectroscopy (XPS), Brunauer–Emmett–Teller (BET) surface area measurement and photoluminescence spectroscopy (PL). Using Cu-Kα radiation ($\lambda = 1.5418$ Å) with scan range 10–70°, XRD patterns were obtained from a X-ray diffractometer (XRD, Bruker, D8 Advance). Morphology of the synthesized materials were analysed by a field emission scanning electron microscope (FESEM, Carl-Zeiss-SIGMA). UV-Vis absorbance spectra in the range of 328 nm to 1000 nm were obtained using a UV-Vis spectrophotometer (JASCO V-530). FTIR spectra of the samples were recorded in the range 400 cm^{-1} to 4000 cm^{-1} by a spectrophotometer (JASCO FT/IR-460-Plus). Al Kα monochromatic X-ray source (VG SCIENTA) with energy 1486.6 eV was used for X-ray energy photoelectron spectroscopy (XPS) measurements along with electron energy analyzer (VG SCIENTAR4000WAL), with total experimental energy resolution better than 0.6 eV at room temperature. The Brunauer–Emmett–Teller (BET) surface area measurements were done by nitrogen adsorption at temperature 77 K using automated gas sorption data acquisition and reduction quantachrome instrument (Quantachrome® ASiQwin™). Room temperature photoluminescence spectra of the samples were recorded using a spectro-fluorometer (Quanta Master 40).

2.4. Photocatalytic experimental set up

The degradation of RB and MO were studied under visible light illumination, using the synthesized samples as photocatalysts. Light from a tungsten lamp (Philips, 200 W) was made to pass through 10 mm deep 1 M solution of $NaNO_2$. The $NaNO_2$ solution was used as UV cut-off filter to get a source of light with wavelength greater than 410 nm, resembling visible light.[59] For each case, a certain amount of dye was added to de-ionised water to get 1×10^{-5} M dye solution. UV-Vis absorption spectrum of the dye solution was taken and in all cases denoted as the UV-Vis spectrum of the dye at zero time (t_0). Adsorption–desorption equilibrium was attained for each sample and each dye by adding 20 mg of sample as photocatalyst into 50 ml dye solution and kept under magnetic stirring for one hour in dark and under ambient temperature and pressure. Then, the solution was placed 10 cm below the tungsten lamp in the above mentioned way to get an optical irradiance of 70 mW cm^{-2}. After switching on the tungsten lamp, UV-Vis spectra of the solution were recorded at given time intervals to study the degradation of dyes in the presence of the prepared samples acting as photocatalysts under the visible light illumination. At given time intervals, 3 ml suspension were sampled and centrifuged to remove the photocatalyst powders. The concentration of dye was analyzed through UV-Vis spectrophotometry.

3. Results and discussions

3.1. Structural characterization

XRD spectra analysis. The XRD spectra of the synthesized samples PSA, PC1, PC2 and PC4 are shown in Fig. 1. Peaks

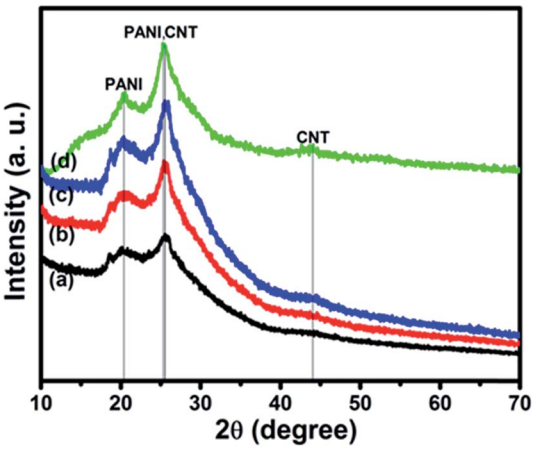

Fig. 1 XRD spectra of (a) PSA, (b) PC1, (c) PC2 and (d) PC4.

around 20° and 25.57° correspond to periodicity perpendicular to and parallel with the polymer backbone chain in PANI respectively.[60,61] XRD peaks of SWCNT occur around 26.2° and 42.7°.[62] In case of composites, peaks are found around the above mentioned peak simplifying that unit structure of PANI has been retained even in the composites.[63]

FESEM images analysis. Fig. 2 shows the FESEM images of PANI and PANI–SWCNT composites. The morphology in Fig. 2(a) reveals polymerization of pure PANI in almost agglomerated form. With the introduction of SWCNTs as in Fig. 2(b–d), some morphological changes take place. FESEM images of the composite show polymerization of PANI over SWCNTs leaving very little PANI in agglomerated form as well as almost no bare SWCNT.

UV-Vis spectra analysis. The normalized UV-Vis spectra of the samples are given in Fig. 3. It is found that there is an absorbance band around 382–390 nm which corresponds to polaron–π transition,[64] the shoulder around 600 nm

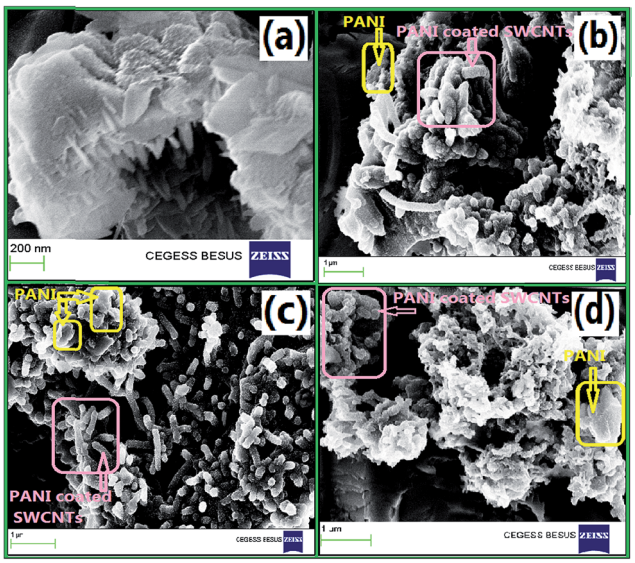

Fig. 2 FESEM images of (a) PSA, (b) PC1, (c) PC2 and (d) PC4.

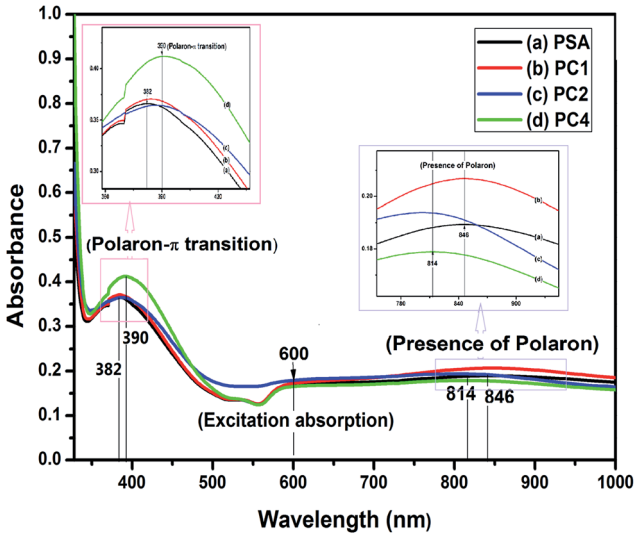

Fig. 3 Normalized UV-Vis spectra of (a) PSA, (b) PC1, (c) PC2 and (d) PC4.

corresponds to exciton absorption of quinoid rings[65] and a band around 846 nm suggests the presence of polaron due to doping in PANI.[66] In composites, the band around 846 nm is found to be blue shifted. It is known that pure SWCNTs have peak around 260 nm [67] and do not have any absorbance peak in the region 600–1000 nm. So the bands found here are due to the presence of PANI and the blue shift is due to the interaction of SWCNTs with PANI in the composites as observed from FTIR spectra discussed in the next section.

FTIR spectra analysis. Fig. 4 represents the FTIR spectra of PANI and its composites (with SWCNT). The peaks of PANI emeraldine salt are observed at 820 cm^{-1} associated with the aromatic C–H bending out of the plane for 1,4 di-substituted benzene ring,[68] 1146 cm^{-1} due to B–NH^{+}=Q stretching, 1348 cm^{-1} and 1384 cm^{-1} due to C–N stretching of secondary

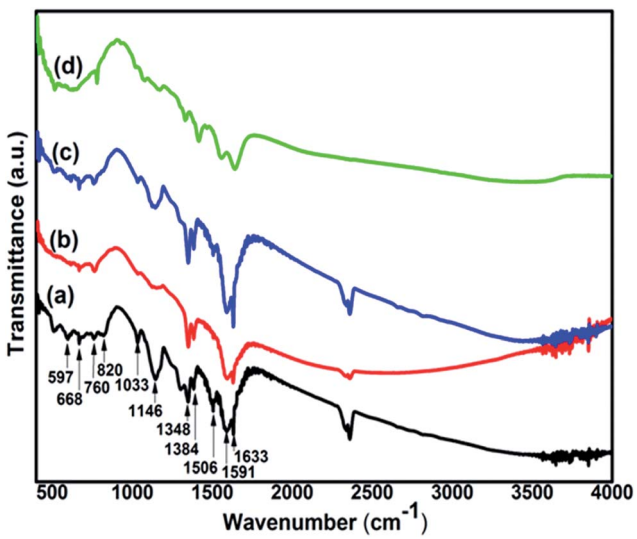

Fig. 4 FTIR spectra of (a) PSA, (b) PC1, (c) PC2 and (d) PC4.

aromatic amine, at 1506 cm^{-1} for benzenoid (B) ring stretching, 1591 cm^{-1} and 1633 cm^{-1} for C=C quinonoid (Q) ring stretching in emeraldine salt and base respectively.[69,70]

The peaks at 597 cm^{-1} due to out-of-plane bending of SSA ring, 668 cm^{-1} attributed to in-plane bending and/or out-of-plane bending of SSA ring, 760 cm^{-1} corresponding to γ_{C-H} vibration of SSA ring and 1033 cm^{-1} due to symmetric stretching of SO_3 group confirm that PANI samples are doped with 5-sulfosalicylate anions of the acid (sulfosalicylic acid).[71–73]

From the FTIR spectra of the composite, it is found that SWCNT interacts with PANI at different reaction sites due to which PANI peaks (Fig. 4(a)) are shifted as has been observed in PANI/nano-SiO_2 [74] and PANI–MWCNT composite.[75] The stretching modes of C–N at 1384 cm^{-1} and C=C at 1506 cm^{-1} and 1633 cm^{-1} are blue shifted to 1416 cm^{-1}, 1557 cm^{-1} and 1643 cm^{-1} respectively. This is an indication of bonds becoming stronger in the composite. Similarly C–C bond at 819 cm^{-1} and C–H bond at 1033 cm^{-1} which are red shifted to 780 cm^{-1} and 1022 cm^{-1} respectively suggests that these bonds become weaker.

XPS analysis. The valence states and the chemical environment of constituent elements on the surface of the PANI–SWCNT composite is explored by X-ray photoelectron spectroscopy (XPS). Fig. 5(a) shows the spectrum of carbon (C 1s) in PC2 having binding energy of 285.5 eV which is close to that of pure PANI (283.9 eV) and SWNT (283.5 eV).[70]

In the spectrum of nitrogen (N 1s), shown in Fig. 5(b), the lowest binding energy at ~399.2 eV suggests the presence of quinoid amine in the backbone of PANI. The peak at ~400 eV is due to the benzenoid di-amine nitrogen of PANI while the higher binding energy at ~401.2 eV represents the positively charged nitrogen ($-N^{\bullet+}$) and the protonated amine ($=N^{\bullet+}$).[76] Fig. 5(c) depicts oxygen (O 1s) spectrum of PC2 with a binding energy peak at ~530.5 eV usually ascribed to C–O or C–OH group in carbon based nanomaterials.[77] The higher binding energy peak at ~532.6 eV could be assigned to bound water molecules.[78]

3.2. Photocatalytic activity study

The characteristic absorptions of RB at $\lambda_{max} = 550$ nm and MO at $\lambda_{max} = 465$ nm were employed to monitor the photocatalytic degradation process.[40,79] In presence of PSA, PC1, PC2 and PC4 as the photocatalysts, Fig. 6(i) and 7(i) are the reaction profiles which show the photodegradation of RB and MO as a function of time, where C_t is the concentration of dye after irradiation and C_0 is the concentration after the adsorption equilibrium on the photocatalyst particles before irradiation. Similarly, in Fig. 6(ii) and 7(ii), the kinetic plots, where the plots of $\ln(C_0/C_t)$ *vs.* irradiation time are shown for RB and MO, respectively. We can see that the degradation process for both the dyes with catalysts follow pseudo first order kinetics. The degradation efficiency and rate constant for RB and MO were calculated from the reaction profiles and kinetic plots in Fig. 6 and 7 using the simple equations as follows:

$$R\% = (1 - C_t/C_0) \times 100 \quad (1)$$

where, $R\%$ is degradation efficiency of RB and MO, C_0 is the initial concentration and C_t is the concentration of RB and MO at different irradiation times, and

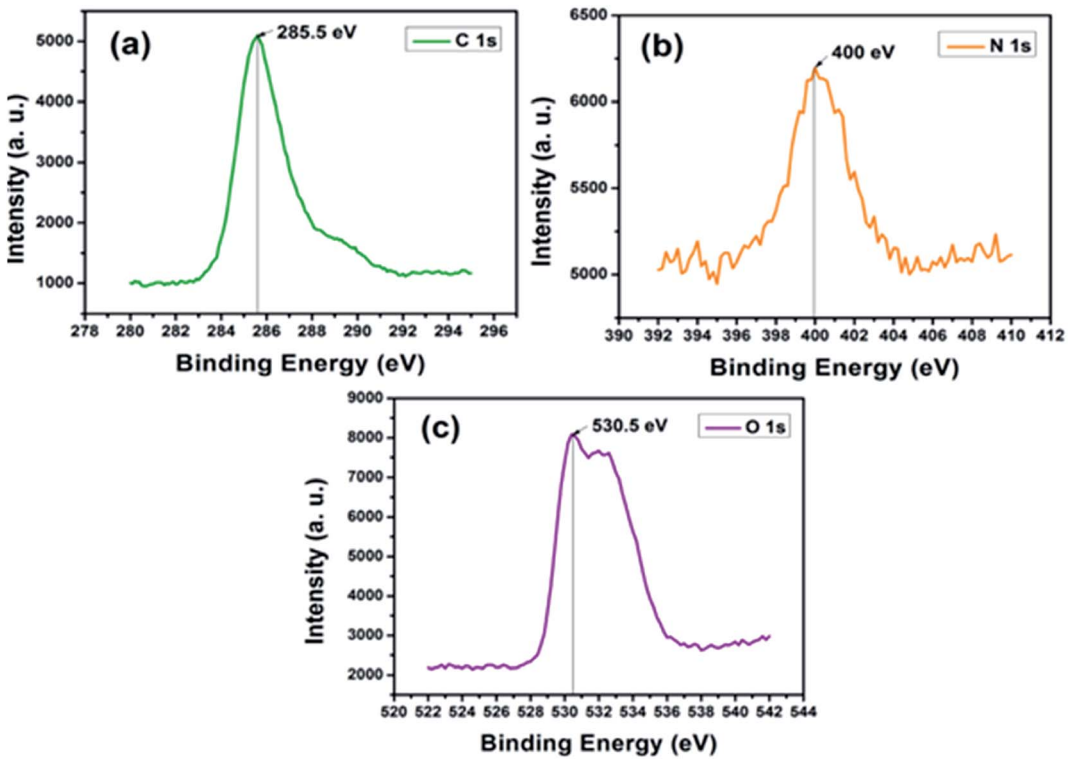

Fig. 5 XPS (a) C 1s (b) N 1s and (c) O 1s XPS core level spectrum of PC2.

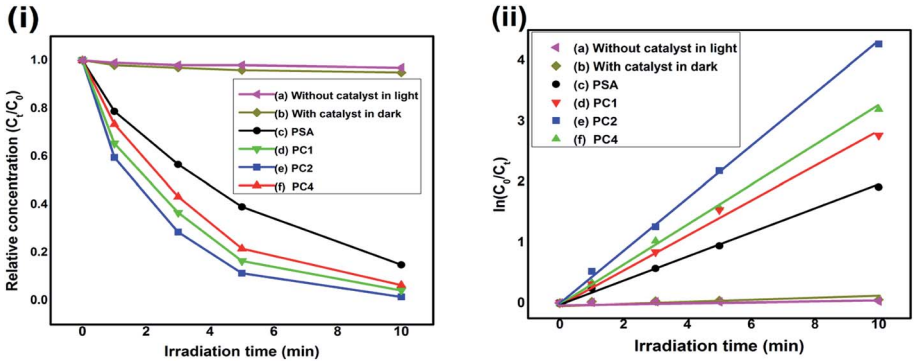

Fig. 6 (i) Reaction profile of RB degradation in an aqueous solution against specific time intervals under various conditions. (ii) First-order kinetic plot of $\ln(C_0/C_t)$ *vs.* irradiation time of RB degradation for (a) without catalyst in light, (b) with catalyst in dark, (c) PSA, (d) PC1, (e) PC2 and (f) PC4.

$$\ln(C_0/C_t) = t \times K_{app} \quad (2)$$

where, K_{app} is pseudo-first order rate constant and t is irradiation time.[80]

Blank tests (dye solution without any photocatalyst) under visible light exhibited very little photolysis, indicating that dyes are stable under visible light. Under identical experimental conditions, PC2 exhibited much enhanced photocatalytic activity. The photodegradation rate of RB and MO reached 98.6% and 94.35% in presence of the PC2 composite after 10 min and 30 min of visible light irradiation, respectively. Only 85.2% and 75.9% of RB and MO were degraded by PSA, indicating that the PANI–SWCNT composite is a superior photocatalyst than SSA doped PANI. The UV-Vis absorption spectral changes of RB and MO dyes in presence of PC2 due to visible light irradiated photo catalysis is given in Fig. ESI-1.†

The slopes of the kinetic plots give the first order rate constants, estimated to be 0.42394 and 0.09505 min^{-1} with PC2 for RB and MO dyes, respectively. A comparison of degradation efficiency (R%) and rate constant (min^{-1}) of the samples acting as photocatalysts for the degradation of RB and MO is presented in Table 2 and Fig. 8 depicts the degradation efficiencies of the samples for various SWCNT content for RB and MO dyes.

To propose the mechanism of the enhanced photocatalytic activity of the PANI–SWCNT composite, the relative band positions of the two semiconductors were compared[81–83] as the band-edge potential levels play a crucial role in determining the flow of photoexcited charge carriers in a coupled heterostructure. The conduction band bottom of PANI is higher than that of SWCNT and the valence band top of PANI is higher than that of SWCNT. The band structure is useful for the separation and transportation of charge carriers. As illustrated in Fig. 9, under visible-light irradiation, both SSA doped PANI and SWCNT are easily excited and electrons and holes are generated. Photogenerated electrons in the SSA doped PANI flows downhill from conduction band of PANI to conduction band of SWCNT because of the intimate contact between the two semiconductors. Simultaneously, holes on the valence band of

Table 2 A comparison of rate constant (K_{app}) and degradation efficiency (R) of the samples acting as photocatalysts for the degradation of RB and MO dyes

	In case of RB		In case of MO	
Sample name	K_{app} (min^{-1})	R (%)	K_{app} (min^{-1})	R (%)
PSA	0.18719	85.2	0.04661	75.9
PC1	0.27757	93.68	0.06905	87.30
PC2	0.42394	98.6	0.09505	94.35
PC4	0.31782	95.91	0.07772	90.34

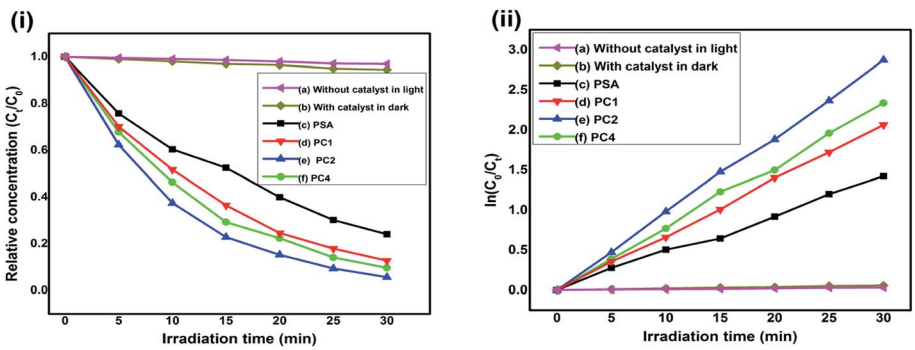

Fig. 7 (i) Reaction profile of MO degradation in an aqueous solution against specific time intervals under various conditions. (ii) First-order kinetic plot of $\ln(C_0/C_t)$ *vs.* irradiation time of MO degradation for (a) without catalyst in light, (b) with catalyst in dark, (c) PSA, (d) PC1, (e) PC2 and (f) PC4.

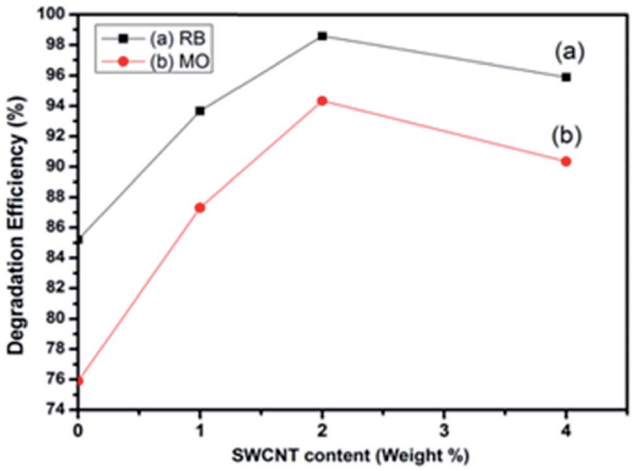

Fig. 8 Degradation efficiency *vs.* SWCNT content of the samples under visible light irradiation for RB and MO dyes.

SWCNT can be transferred to that of PANI under the band energy potential difference. In this way, the photogenerated electrons and holes can be efficiently separated and the recombination of electron–hole pairs can be reduced. Electrons present in conduction bands of both SWCNT and doped PANI can react with dissolved O_2 to form superoxide radical anions ($^{\bullet}O_2^-$) as both of them lies above the reduction potential of $O_2/^{\bullet}O_2^-$.[81–84] Further reduction of superoxide radical anion gives hydroxyl radical.[20] On the other hand, dye molecules absorb light and get photoexcited. Photogenerated electrons in dyes can flow downhill from LUMO to the CB of SWCNT and enhance the photodegradation rate.[47,85] The active species like $^{\bullet}O_2^-$ and $^{\bullet}OH$ react with dye cation and forms colorless small degraded products. Direct oxidative attack on dye molecules by holes can also occur.[86]

To ascertain the role of active species, including hole (h^+), electron (e^-), hydroxyl radical ($^{\bullet}OH$) and super-oxide radical ($^{\bullet}O_2^-$), corresponding scavengers of them were added in the reaction medium. This is crucial for elucidating the photocatalytic mechanism. As shown in Fig. 10, different scavengers have different effects on the degradation of MO and RB, respectively. The addition of $^{\bullet}OH$, e^-, h^+ and $^{\bullet}O_2^-$ scavengers induce great change in MO and RB photodegradation, indicating role of all of them. The possible mechanism involves the following steps[20]

$$\text{SSA doped PANI} \xrightarrow{h\nu} (h_{VB}^{+} + e_{CB}^{-})\ \text{SSA doped PANI} \quad (1)$$

$$\text{SWCNT} \xrightarrow{h\nu} (h_{VB}^{+} + e_{CB}^{-})\ \text{SWCNT} \quad (2)$$

$$\text{Dye} \xrightarrow{h\nu} \text{dye}^{*} \quad (3)$$

$$\text{Dye}^{*} \rightarrow \text{dye}^{+} + (e_{CB}^{-})\ \text{SWCNT} \quad (4)$$

$$\text{Dye}^{*} + (h_{VB}^{+})\ \text{SWCNT/SSA doped PANI} \rightarrow \text{dye}^{+} \quad (5)$$

$$(e_{CB}^{-})\ \text{SWCNT/SSA doped PANI} + O_2 \rightarrow {}^{\bullet}O_2^- \quad (6)$$

$${}^{\bullet}O_2^- + 2e_{CB}^{-} + 2H^+ \rightarrow {}^{\bullet}OH + OH^- \quad (7)$$

$${}^{\bullet}OH + {}^{\bullet}O_2^- + \text{dye}^{+} \rightarrow \text{colourless degraded products} \quad (8)$$

$$\text{Dye} + (h_{VB}^{+})\ \text{SWCNT/SSA doped PANI} \rightarrow \text{colourless degraded products} \quad (9)$$

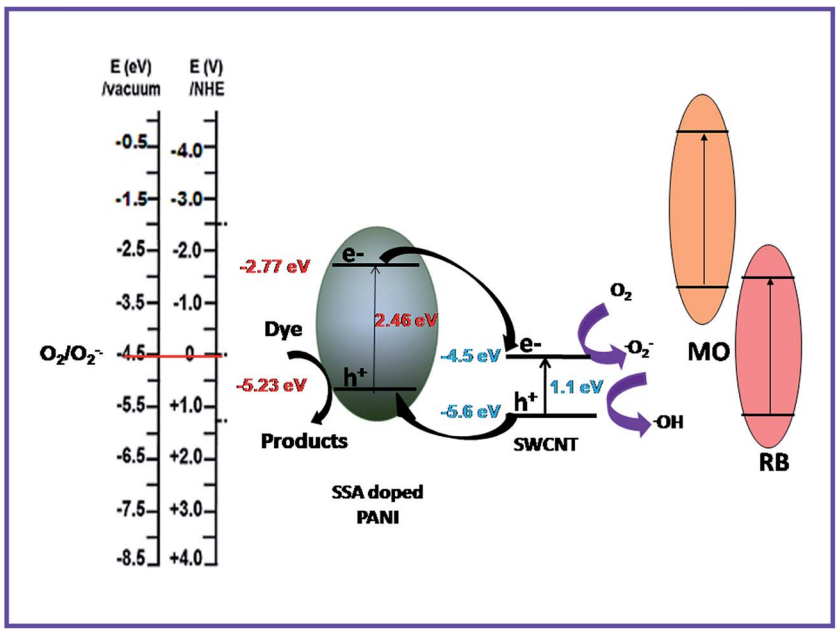

Fig. 9 Proposed mechanism of PANI–SWCNT structure for charge transfer of the photogenerated electrons and holes under visible light illumination.

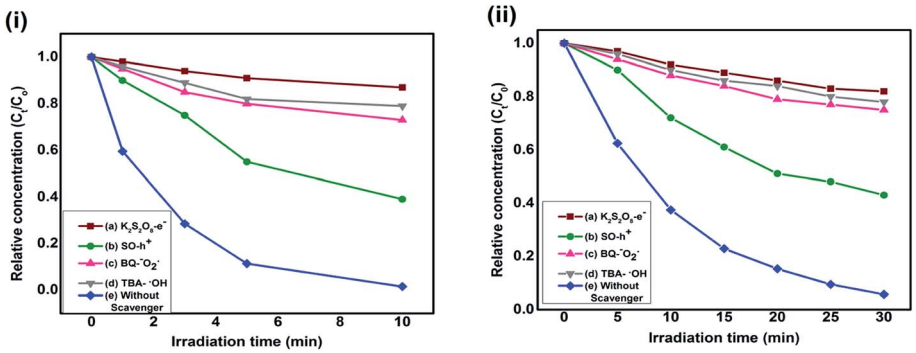

Fig. 10 Reaction profile of photocatalytic degradation of (i) RB and (ii) MO as a function of irradiation time in presence of PC2 and different scavengers.

The stability of PC2 has been further investigated by recycling the photocatalyst and the relative dye concentration *versus* irradiation time for four consecutive cycles is shown in Fig. 11(a) for RB and MO dye degradation. The degradation efficiency of RB solution was found to be more than 94% after 4 cycles, while for MO solution it is 92% as shown in Fig. 11(b).

3.3. BET surface area and pore size analysis

Fig. 12(a) shows isotherm adsorption/desorption curve with relative pressure for PSA and PC2 and it is seen that adsorption/desorption is greater for composite (PC2) than pure PANI. The surface area for pure PANI (PSA) is 24.9 m^2 g^{-1} and for composite (PC2) it is 31 m^2 g^{-1} which matches with reported result.[87] As seen in FESEM images, SWCNTs hinder agglomeration of PANI, which leads to increase the surface area in the composite. Cumulative and differential pore volume distribution with pore width are shown in Fig. 12(b) and (c) respectively by using Barrett–Joyner–Halenda (BJH) desorption data. For composite, higher pore volume is observed which is a signature of more porous morphology.

3.4. Photoluminescence (PL) property

Fluorescence intensity in the PL spectra provides the information regarding the recombination efficiency of photogenerated electrons and holes of a material. Higher recombination rate of photogenerated electrons and holes produces strong fluorescence intensity. That means these photo generated carriers have lower lifetime. However if the recombination rate is low due to high separation efficiency leading to a longer lifetime of the photogenerated carriers, the fluorescence intensity diminishes.

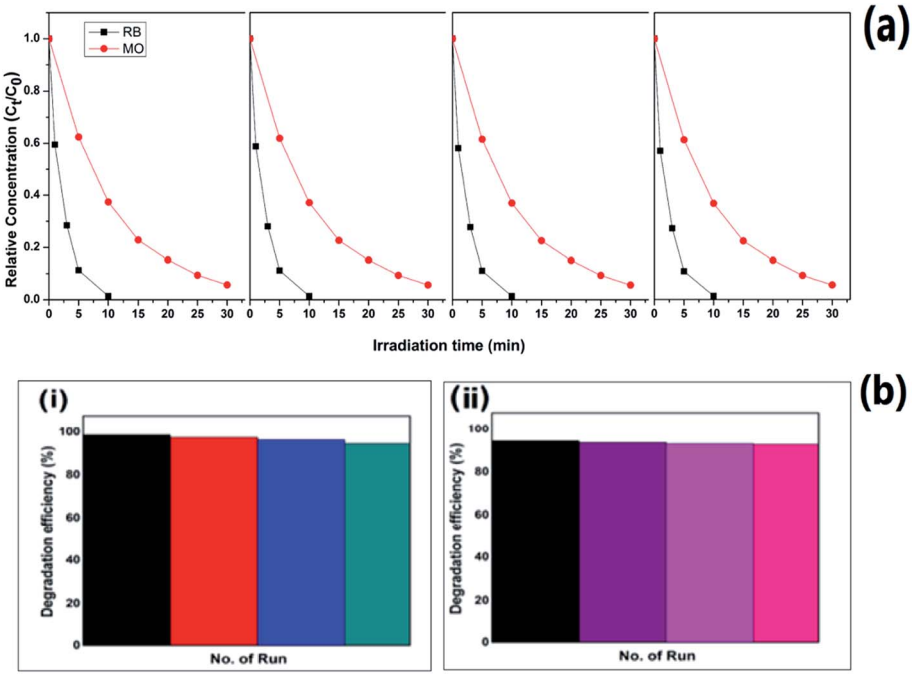

Fig. 11 (a) Relative dye concentration and (b) degradation efficiencies of PC2 with irradiation time for four consecutive cycles of operation for (i) RB and (ii) MO dye.

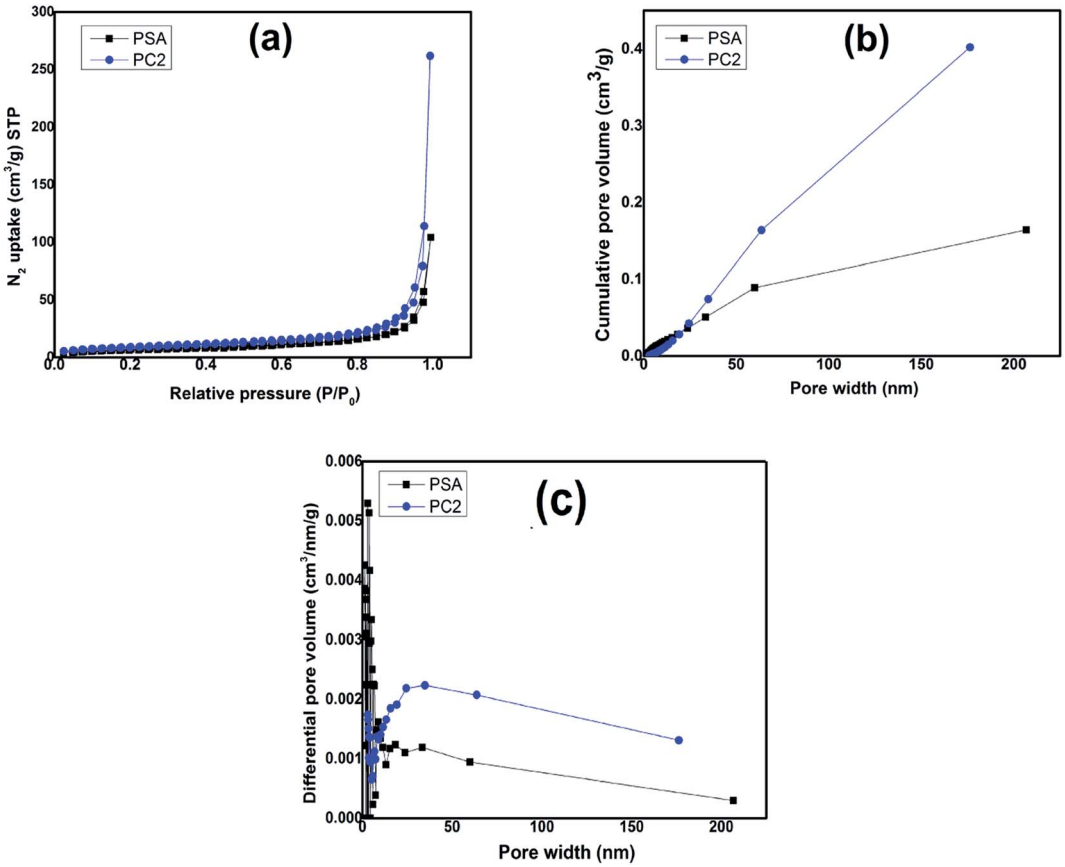

Fig. 12 (a) Isotherms, (b) cumulative and (c) differential pore volume for PSA and PC2.

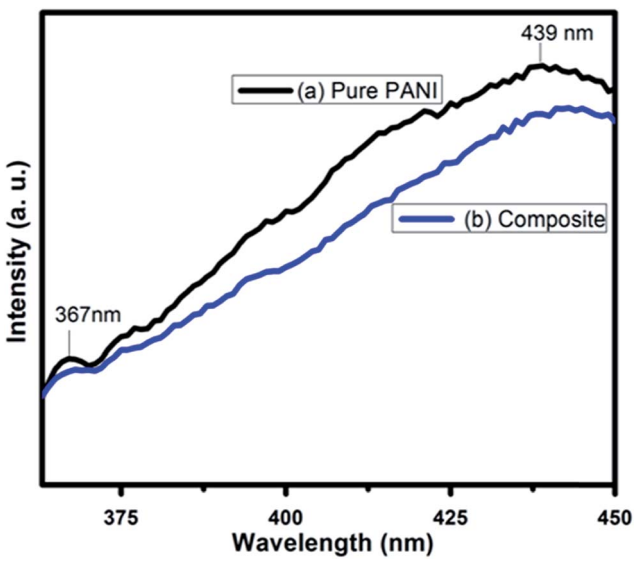

Fig. 13 PL spectra of (a) pure PANI and (b) composite (PC2) at room temperature.

Fig. 13 shows the photoluminescence spectroscopy of PANI and PC2 for excitation wavelength 330 nm. The peaks at 367 nm and 439 nm are clearly due to the π^*–π transition and polaronic band in PANI respectively.[88,89]

In case of composite with 2% SWCNT (PC2), the intensity of these peaks are lowered suggesting improved separation efficiency and life time of the photogenerated electrons and holes in presence of SWCNT. This result supports the experimental observations – the enhanced rate constant and efficiency of photocatalytic degradation of RB and MO dyes under visible light illumination using PANI–SWCNT composite over pure PANI as photocatalyst. The electron hole pairs with longer lifetime are advantageous for creating more of photoreactive species with strong oxidation capabilities, such as O_2^- and $^{\bullet}OH$, which explains for higher photocatalytic activity of PANI–SWCNT composite than pure PANI.[90]

4. Conclusion

SSA doped PANI and PANI–SWCNT composites with different SWCNT content ratio have been synthesized by *in situ* polymerization technique which exhibit highly efficient visible-light-driven photocatalytic activity for the degradation of RB and MO dyes. The structure, surface morphology, valence states and chemical environment of constituent elements on the surface of the samples have been examined and discussed in detail. SWCNT improves the surface area and increases the visible light absorption ability of the composite photocatalyst. Due to the synergistic effect between PANI and SWCNT, the composite displayed an efficient visible-light-responsive

photocatalytic activity as compared to pure PANI through an improved photogenerated carrier separation in the composite. The composite PC2 (2% SWCNT) exhibited the highest photocatalytic performance with a higher rate constant ~2.3 times for RB and ~2 times for MO than that of pure PANI. A possible photocatalytic mechanism on the enhancement of visible light performance of composite over pure PANI is discussed based on the active species trapping experiment.

Acknowledgements

M. J. Chatterjee acknowledges Indian Institute of Engineering Science and Technology, Shibpur for Institute Fellowship. A. Ghosh is thankful to University Grants Commission (INDIA) for her SRF-NET fellowship. CEGESS, IIEST, Shibpur and UGC-DAE Consortium for Scientific Research, Kolkata Centre are acknowledged for providing FESEM and XRD spectra measurements facilities, respectively. Dr Krishnakumar S. R. Menon, Surface Physics Division, SINP is acknowledged for providing XPS data. Ms Mousumi Majumder of CGCRI, Kolkata, is acknowledged for providing the data for BET analysis.

References

1 X. Li, S. Ouyang, N. Kikugawa and J. Ye, Novel Ag_2ZnGeO_4 photocatalyst for dye degradation under visible light irradiation, *Appl. Catal., A*, 2008, **334**, 51–58.

2 S. Ameen, H.-K. Seo, M. Shaheer Akhtar and H. S. Shin, Novel graphene/polyaniline nanocomposites and its photocatalytic activity toward the degradation of Rose Bengal dye, *Chem. Eng. J.*, 2012, **210**, 220–228.

3 M. Mitra, A. Ghosh, A. Mondal, K. Kargupta, S. Ganguly and D. Banerjee, Facile synthesis of aluminium doped zinc oxide–polyaniline hybrids for photoluminescence and enhanced visible-light assisted photo-degradation of organic contaminants, *Appl. Surf. Sci.*, 2017, **402**, 418–428.

4 A. Olad, S. Behboudi and A. A. Entezami, Preparation, characterization and photocatalytic activity of TiO_2/polyaniline core–shell nanocomposite, *Bull. Mater. Sci.*, 2012, **35**(5), 801–809.

5 Y. Lin, D. Li, J. Hu, G. Xiao, J. Wang, W. Li and X. Fu, Highly efficient photocatalytic degradation of organic pollutants by PANI modified TiO_2 composite, *J. Phys. Chem. C*, 2012, **116**, 5764–5772.

6 D. Wang, Y. Wang, X. Li, Q. Luo, J. An and J. Yue, Sunlight photocatalytic activity of polypyrrole–TiO_2 nanocomposites prepared by '*in situ*' method, *Catal. Commun.*, 2008, **9**, 1162–1166.

7 Y. Zhu, S. Xu and D. Yi, Photocatalytic degradation of methyl orange using polythiophene/titanium dioxide composites, *React. Funct. Polym.*, 2010, **70**, 282–287.

8 S. Xu, Y. Zhu, L. Jiang and Y. Dan, Visible light induced photocatalytic degradation of methyl orange by polythiophene/TiO_2 composite particles, *Water, Air, Soil Pollut.*, 2010, **213**, 151–159.

9 S. Shahabuddin, N. Muhamad Sarih, S. Mohamad and S. Nor Atika Baharin, Synthesis and characterization of Co_3O_4 nanocube doped polyaniline nanocomposites with enhanced methyl orange adsorption from aqueous solution, *RSC Adv.*, 2016, **6**, 43388–43400.

10 S. Ameen, M. S. Akhtar, Y. S. Kim, O.-B. Yang and H.-S. Shin, An effective nanocomposite of polyaniline and ZnO: preparation, characterizations and its photocatalytic activity, *Colloid Polym. Sci.*, 2011, **289**, 415–421.

11 V. Eskizeybek, F. Sari, H. Gulce, A. Gulce and A. Avci, Preparation of the new polyaniline/ZnO nanocomposite and its photocatalytic activity for degradation of methylene blue and malachite green dyes under UV and natural sun lights irradiations, *Appl. Catal., B*, 2012, **119–120**, 197–206.

12 H. Zhang, R. Zong and Y. Zhu, Photocorrosion inhibition and photoactivity enhancement for zinc oxide *via* hybridization with monolayer polyaniline, *J. Phys. Chem. C*, 2009, **113**, 4605–4611.

13 H. Zhang, R. Zong, J. Zhao and Y. Zhu, Dramatic visible photocatalytic degradation performances due to synergetic effect of TiO_2 with PANI, *Environ. Sci. Technol.*, 2008, **42**, 3803–3807.

14 M. Radoičić, Z. Šaponjić, I. A. Janković, G. Ćirić-Marjanović, S. P. Ahrenkiel and M. I. Čomor, Improvements to the photocatalytic efficiency of polyaniline modified TiO_2 nanoparticles, *Appl. Catal., B*, 2013, **136–137**, 133–139.

15 F. Wang and S. X. Min, TiO_2/polyaniline composites: an efficient photocatalyst for the degradation of methylene blue under natural light, *Chin. Chem. Lett.*, 2007, **18**, 1273–1277.

16 M. O. Ansari, M. M. Khan, S. A. Ansari, K. Raju, J. Lee and M. H. Cho, Enhanced thermal stability under DC electrical conductivity retention and visible light activity of Ag/TiO_2@polyaniline nanocomposite film, *ACS Appl. Mater. Interfaces*, 2014, **6**, 8124–8133.

17 M. O. Ansari, M. M. Khan, S. A. Ansari, K. Raju, J. Lee and M. H. Cho, Enhanced thermoelectric behaviour and visible light activity of Ag@TiO_2/polyaniline nanocomposite synthesized by biogenic-chemical route, *RSC Adv.*, 2014, **4**, 23713–23719.

18 H. A. Ghaly, A. S. El-Kalliny, T. A. Gad-Allah, N. E. A. Abd El-Sattar and E. R. Souaya, Stable plasmonic Ag/AgCl–polyaniline photoactive composite for degradation of organic contaminants under solar light, *RSC Adv.*, 2017, **7**, 12726–12736.

19 M. R. Patil and V. S. Shrivastava, Photocatalytic degradation of carcinogenic methylene blue dye by using polyaniline–nickel ferrite nano-composite, *Der Chemica Sinica*, 2014, **5**(2), 8–17.

20 L. Ge, C. Han and J. Liu, *In situ* synthesis and enhanced visible light photocatalytic activities of novel PANI-*g*-C_3N_4 composite photocatalysts, *J. Mater. Chem.*, 2012, **22**, 11843–11850.

21 M. Sangareswari and M. Meenakshi Sundaram, Development of efficiency improved polymer-modified TiO_2 for the photocatalytic degradation of an organic dye from wastewater environment, *Appl. Water Sci.*, 2015, 1–10.

22 V. Lakshmi Prasanna and V. Rajagopalan, A new synergetic nanocomposite for dye degradation in dark and light, *Sci. Rep.*, 2016, **6**, 38606.

23 T. Abdiryim, A. Ali, R. Jamal, Y. Osman and Y. Zhang, A facile solid-state heating method for preparation of poly(3,4-ethelenedioxythiophene)/ZnO nanocomposite and photocatalytic activity, *Nanoscale Res. Lett.*, 2014, **9**, 89–96.

24 Y. Bu and Z. Chen, Role of polyaniline on the photocatalytic degradation and stability performance of the polyaniline/silver/silver phosphate composite under visible light, *ACS Appl. Mater. Interfaces*, 2014, **6**, 17589–17598.

25 M. Shang, W. Wang, S. Sun, J. Ren, L. Zhou and L. Zhang, Efficient visible light-induced photocatalytic degradation of contaminant by spindle-like PANI/$BiVO_4$, *J. Phys. Chem. C*, 2009, **113**, 20228–20233.

26 T. S. Anirudhan and S. R. Rejeena, Photocatalytic degradation of eosin yellow using poly(pyrrole-*co*-aniline)-coated TiO_2/nanocellulose composite under solar light irradiation, *J. Mater.*, 2015, 636409.

27 U. Riaz, S. M. Ashraf and M. Aqib, Microwave-assisted degradation of acid orange using a conjugated polymer, polyaniline, as catalyst, *Arabian J. Chem.*, 2014, **7**, 79–86.

28 R. Tanwar, S. Kumar and U. K. Mandal, Photocatalytic activity of PANI/Fe^0 doped BiOCl under visible light-degradation of Congo red dye, *J. Photochem. Photobiol., A*, 2017, **333**, 105–116.

29 M. M. Ayad and A. A. El-Nasr, Adsorption of cationic dye (methylene blue) from water using polyaniline nanotubes base, *J. Phys. Chem. C*, 2010, **114**, 14377–14383.

30 E. T. Kang, K. G. Neoh and K. L. Tan, Polyaniline: a polymer with many interesting intrinsic redox states, *Prog. Polym. Sci.*, 1998, **23**, 277–324.

31 Y. Shirota and H. Kageyama, Charge carrier transporting molecular materials and their applications in devices, *Chem. Rev.*, 2007, **107**, 953–1010.

32 H. Huang, Y. Liu, S.-T. Lee and Z. Kang, Polymer (polyanilines) nanoparticles: a superior catalyst for hydrocarbon selective oxidation, *J. Mater. Chem.*, 2012, **22**, 337–340.

33 Y. T. Ong, A. L. Ahmad, S. H. S. Zein and S. H. Tan, A review on carbon nanotubes in an environmental protection and green engineering perspective, *Braz. J. Chem. Eng.*, 2010, **27**(2), 227–242.

34 D. Zhao, W. Zhang, C. Chen and X. Wang, Adsorption of methyl orange dye onto multiwalled carbon nanotubes, *Procedia Environ. Sci.*, 2013, **18**, 890–895.

35 F. K. Mohamad Alosfur, M. H. Haji Jumali, S. Radiman, N. J. Ridha and A. A. Umar, Visible light photocatalytic activity of TiO_2/MWCNTs nanocomposite prepared using modified microwave technique, *Seventh International Conference on Sensing Technology*, (2013), pp. 777–781.

36 K. Hemalatha, P. Masthanaiah Ette, G. Madras and K. Ramesha, Visible light assisted photocatalytic degradation of organic dyes on TiO_2–CNT nanocomposites, *J. Sol-Gel Sci. Technol.*, 2015, **73**, 72–82.

37 K. Wu, J. Yu and X. Jiang, Multi-walled carbon nanotubes modified by polyaniline for the removal of alizarin yellow R from aqueous solutions, *Adsorpt. Sci. Technol.*, 2017, 1–17.

38 A. T. Kuvarega and B. B. Mamba, Double walled carbon nanotube/TiO_2 nanocomposites for photocatalytic dye degradation, *J. Nanomater.*, 2016, 3746861.

39 R. Kumar, M. Omaish Ansari and M. A. Barakat, DBSA doped polyaniline/multi walled carbon nanotubes composite for high efficiency removal of Cr(VI) from aqueous solution, *Chem. Eng. J.*, 2013, **228**, 748–755.

40 R. Kumawat, I. Bhati and R. Ameta, Role of some metal ions in photocatalytic degradation of Rose Bengal dye, *Indian J. Chem. Technol.*, 2012, **19**, 191–194.

41 A. Ghosh and A. Mondal, A simple electrochemical route to deposit Cu_7S_4 thin films and their photocatalytic properties, *Appl. Surf. Sci.*, 2015, **328**, 63–70.

42 A. Ghosh, M. Mitra, D. Banerjee and A. Mondal, Facile electrochemical deposition of Cu_7Te_4 thin films with visible-light driven photocatalytic activity and thermoelectric performance, *RSC Adv.*, 2016, **6**, 22803–22811.

43 A. Ghosh and A. Mondal, Fabrication of stable, efficient and recyclable p-CuO/n-ZnO thin film heterojunction for visible light driven photocatalytic degradation of organic dyes, *Mater. Lett.*, 2016, **164**, 221–224.

44 N. Mittal, A. Shah, P. B. Punjabi and V. K. Sharma, Photodegradation of rose bengal using MnO_2 (manganese dioxide), *Rasayan J. Chem.*, 2009, **2**(2), 516–520.

45 J. Guo, X. Chen, Y. Shi, Y. Lan and C. Qin, Rapid photodegradation of methyl orange (MO) assisted with Cu(II) and tartaric acid, *PLoS One*, 2015, **10**(8), e0134298.

46 W. Szeto, C. Wai Kan, C. W. M. Yuen, S.-W. Chan and K. H. Lam, Effective photodegradation of methyl orange using fluidized bed reactor loaded with cross-linked chitosan embedded nano-CdS photocatalyst, *Int. J. Chem. Eng.*, 2014, 270946.

47 T. A. Saleh, A. A. Al-Saadi and V. K. Gupta, Carbonaceous adsorbent prepared from waste tires: experimental and computational evaluations of organic dye methyl orange, *J. Mol. Liq.*, 2014, **191**, 85–91.

48 N. Cheng, J. Tian, Q. Liu, C. Ge, A. H. Qusti, A. M. Asiri, A. O. Al-Youbi and X. Sun, Au-nanoparticle-loaded graphitic carbon nitride nanosheets: green photocatalytic synthesis and application toward the degradation of organic pollutants, *ACS Appl. Mater. Interfaces*, 2013, **5**, 6815–6819.

49 S. Ghosh, N. Amoin Kouame, S. Remita, L. Ramos, F. Goubard, P.-H. Aubert, A. Dazzi, A. Deniset-Besseau and H. Remita, Visible-light active conducting polymer nanostructures with superior photocatalytic activity, *Sci. Rep.*, 2015, **5**, 18002.

50 Z. Pei, L. Ding, M. Lu, Z. Fan, S. Weng, J. Hu and P. Liu, Synergistic effect in polyaniline-hybrid defective ZnO with enhanced photocatalytic activity and stability, *J. Phys. Chem. C*, 2014, **118**, 9570–9577.

51 Yi-J. Xu, Y. Zhuang and X. Fu, New insight for enhanced photocatalytic activity of TiO_2 by doping carbon nanotubes: a case study on degradation of benzene and methyl orange, *J. Phys. Chem. C*, 2010, **114**, 2669–2676.

52 Y. Zhu and Y. Dan, Photocatalytic activity of poly(3-hexylthiophene)/titanium dioxide composites for degrading methyl orange, *Sol. Energy Mater. Sol. Cells*, 2010, **94**, 1658–1664.

53 Y. Su, Y. Yang, H. Zhang, Y. Xie, Z. Wu, Y. Jiang, N. Fukata, Y. Bando and Z. L. Wang, Enhanced photodegradation of methyl orange with TiO_2 nanoparticles using a triboelectric nanogenerator, *Nanotechnology*, 2013, **24**, 295401.

54 R. Zha, R. Nadimicherla and X. Guo, Ultraviolet photocatalytic degradation of methyl orange by nanostructured TiO_2/ZnO heterojunctions, *J. Phys. Chem. A*, 2015, **3**, 6565–6574.

55 P. Niu, Photocatalytic degradation of methyl orange in aqueous TiO_2 suspensions, *Asian J. Chem.*, 2013, **25**(2), 1103–1106.

56 Y. Li, X. Li, J. Li and J. Yin, Photocatalytic degradation of methyl orange by TiO_2-coated activated carbon and kinetic study, *Water Res.*, 2006, **40**, 1119–1126.

57 H. Zhang, P. Xu, G. Du, Z. Chen, K. Oh, D. Pan and Z. Jiao, A facile one-step synthesis of TiO_2/graphene composites for photodegradation of methyl orange, *Nano Res.*, 2011, **4**(3), 274–283.

58 M. J. Chatterjee, D. Banerjee and K. Chatterjee, Composite of single walled carbon nanotube and sulfosalicylic acid doped polyaniline: a thermoelectric material, *Mater. Res. Express*, 2016, **3**, 085009.

59 M. Ikbal, R. Banerjee, S. Atta, D. Dhara, A. Anoop and N. D. Pradeep Singh, Synthesis, photophysical and photochemical properties of photoacid generators based on *N*-hydroxyanthracene-1,9-dicarboxyimide and their application toward modification of silicon surfaces, *J. Org. Chem.*, 2012, **77**, 10557–10567.

60 H. K. Chaudhari and D. S. Kelkar, Investigation of structure and electrical conductivity in doped polyaniline, *Polym. Int.*, 1997, **42**, 380–384.

61 J. P. Pouget, M. E. Jdzefowiczt, A. J. Epstein, X. Tang and A. G. MacDiarmid, X-ray structure of polyaniline, *Macromolecules*, 1991, **24**, 779–789.

62 O. Zhou, R. M. Fleming, D. W. Murphy, C. H. Chen, R. C. Haddon, A. P. Ramirez and S. H. Glarum, Defects in carbon nanostructures, *Science*, 1994, **263**(25), 1744–1747.

63 M. Mitra, C. Kulsi, K. Chatterjee, K. Kargupta, S. Ganguly, D. Banerjee and S. Goswami, Reduced graphene oxide-polyaniline composites—synthesis, characterization and optimization for thermoelectric applications, *RSC Adv.*, 2015, **5**, 31039–31048.

64 T.-M. Wu, Y.-W. Lin and C.-S. Lia, Preparation and characterization of polyaniline/multi-walled carbon nanotube composites, *Carbon*, 2005, **43**, 734–740.

65 S. Ding, H. Mao and W. Zhang, Fabrication of DBSA-doped polyaniline nanorods by interfacial polymerization, *J. Appl. Polym. Sci.*, 2008, **109**, 2842–2847.

66 H. Xia and Q. Wang, Preparation of conductive polyaniline/nanosilica particle composites through ultrasonic irradiation, *J. Appl. Polym. Sci.*, 2003, **87**, 1811–1817.

67 T. T. Nguyen, Sy U. Nguyen, D. T. Phuong, D. C. Nguyen and A. T. Mai, Dispersion of denatured carbon nanotubes by using a dimethylformamide solution, *Adv. Nat. Sci.: Nanosci. Nanotechnol.*, 2011, **2**, 035015.

68 R. Cruz-Silva, J. Romero-García, J. L. Angulo-Sánchez, E. Flores-Loyola, M. H. Farías, F. F. Castillón and J. A. Díaz, Comparative study of polyaniline cast films prepared from enzymatically and chemically synthesized polyaniline, *Polymer*, 2004, **45**, 4711–4717.

69 X. B. Yan, Z. J. Han, Y. Yang and B. K. Tay, NO_2 gas sensing with polyaniline nanofibers synthesized by a facile aqueous/organic interfacial polymerization, *Sens. Actuators, B*, 2007, **123**, 107–113.

70 M. R. Karim, C. J. Lee, Y.-T. Park and Mu S. Lee, SWNTs coated by conducting polyaniline: synthesis and modified properties, *Synth. Met.*, 2005, **151**, 131–135.

71 G. Socrates, *Infrared and Raman Characteristic Group Frequencies: Tables and Charts of Work*, Wiley, Chichester, NY, 2001, vol. 107, (221), pp. 94–99.

72 D. C. Trivedi and S. K. Dhawan, Investigations on the effect of 5-sulfosalicylic acid on the properties of polyaniline, *Synth. Met.*, 1993, **58**, 309–324.

73 H. T. Varghese, C. Y. Panicker and D. Philip, IR, Raman and SERS spectra of 5-sulphosalicylic acid dihydrate, *J. Raman Spectrosc.*, 2007, **38**, 309–315.

74 X. Lia, G. Wang and X. Li, Surface modification of nano-SiO_2 particles using polyaniline, *Surf. Coat. Technol.*, 2005, **197**, 56–60.

75 R. Chan Yu King, F. Roussel, J.-F. Brun and C. Gors, Carbon nanotube–polyaniline nanohybrids: influence of the carbon nanotube characteristics on the morphological, spectroscopic, electrical and thermoelectric properties, *Synth. Met.*, 2012, **162**, 1348–1356.

76 K. Zhang, L. L. Zhang, X. S. Zhao and J. Wu, Graphene/polyaniline nanofiber composites as supercapacitor electrodes, *Chem. Mater.*, 2010, **22**, 1392–1401.

77 O. Akhavan, The effect of heat treatment on formation of graphene thin films from graphene oxide, *Carbon*, 2010, **48**, 509–519.

78 D. Yang, A. Velamakanni, G. Bozoklu, S. Park, M. Stoller, R. D. Piner, S. Stankovich, I. Jung, D. A. Field, C. A. Ventrice and R. S. Ruoff, Chemical analysis of graphene oxide films after heat and chemical treatments by X-ray photoelectron and micro-Raman spectroscopy, *Carbon*, 2009, **47**, 145–152.

79 X.-F. Lu, H.-R. Ma, Q. Zhang and K. Du, Degradation of methyl orange by UV, O_3 and UV/O_3 systems: analysis of the degradation effects and mineralization mechanism, *Res. Chem. Intermed.*, 2013, **39**, 4189–4203.

80 D. Dong, P. Li, X. Li, Q. Zhao, Y. Zhang, C. Jia and P. Li, Investigation on the photocatalytic degradation of pyrene on soil surfaces using nanometer anatase TiO_2 under UV irradiation, *J. Hazard. Mater.*, 2010, **174**, 859–863.

81 H.-Y. Si, C.-H. Liu, H. Xu, T.-M. Wang and H.-L. Zhang, Shell-Controlled Photoluminescence in CdSe/CNT Nanohybrids, *Nanoscale Research Letters*, 2009, **4**, 1146–1152.

82 T. Guo, L. Wang, D. G. Evans and W. Yang, Synthesis and photocatalytic properties of a polyaniline-intercalated layered protonic titanate nanocomposite with a p–n

heterojunction structure, *J. Phys. Chem. C*, 2010, **114**, 4765–4772.

83 Y. Xiao, G. Han, Y. Chang, H. Zhou, M. Li and Y. Li, An all-solid-state perovskite-sensitized solar cell based on the dual function polyaniline as the sensitizer and p-type hole-transporting material, *J. Power Sources*, 2014, **267**, 1–8.

84 P. S. Rao and E. Hayon, Redox potentials of free radicals. IV. Superoxide and hydroperoxy radicals $^{\bullet}O_2^-$ and $^{\bullet}HO_2$, *J. Phys. Chem.*, 1975, **79**(4), 397–402.

85 T. Oku, N. Kakuta, K. Kobay ashi, A. Suzuki and K. Kikuchi, Fabrication and characterization of TiO_2-based dye-sensitized solar cells, *Prog. Nat. Sci.: Mater. Int.*, 2011, **21**, 122–126.

86 M. Rochkind, S. Pasternak and Y. Paz, Using dyes for evaluating photocatalytic properties: a critical review, *Molecules*, 2015, **20**, 88–110.

87 E. N. Konyushenko, J. Stejskal, M. Trchová, J. Hradil, J. Kovářová, J. Prokeš, M. Cieslar, J.-Y. Hwang, K.-H. Chen and I. Sapurina, Multi-wall carbon nanotubes coated with polyaniline, *Polymer*, 2006, **47**, 5715–5723.

88 D. Geethalakshmi, N. Muthukumarasamy and R. Balasundaraprabhu, Effect of dopant concentration on the properties of HCl-doped PANI thin films prepared at different temperatures, *Optik*, 2014, **125**, 1307–1310.

89 R. K. Agrawalla, R. Paul, A. K. Chakraborty and A. K. Mitra, Synthesis and optical characterization of sulfonated polyaniline/single-walled carbon nanotube/zinc sulphide nanocomposite, *ISRN Nanotechnol.*, 2013, 253016.

90 Y. Long, Y. Lu, Y. Huang, Y. Peng, Y. Lu, S.-Z. Kang and J. Mu, Effect of C_{60} on the photocatalytic activity of TiO_2 nanorods, *J. Phys. Chem. C*, 2009, **113**, 13899–13905.